First-principles investigation of the origin of superconductivity in $TlBi_2$

Aiqin Yang, Xiangru Tao, Yundi Quan,* and Peng Zhang†
MOE Key Laboratory for Non-Equilibrium Synthesis and Modulation of Condensed Matter, Shanxi Province Key Laboratory of Advanced Functional Materials and Mesoscopic Physics, School of Physics, Xi'an Jiaotong University, 710049 Xi'an, Shaanxi, People's Republic of China

(Received 21 May 2023; accepted 20 July 2023; published 21 August 2023)

The intermetallic compound $TlBi_2$ crystallizes in the MgB_2 structure and becomes superconducting below 6.2 K. Considering that both Tl and Bi have heavy atomic masses, it is puzzling why $TlBi_2$ is a conventional phonon-mediated superconductor. We have performed comprehensive first-principles calculations of the electronic structures, the phonon dispersions, and the electron-phonon couplings for $TlBi_2$. The $6p$ orbitals of bismuth dominate over the states near the Fermi level, forming strong intralayer $p_{x/y}$ and interlayer p_z σ bonds which are known to have strong electron-phonon coupling. In addition, the large spin-orbit coupling interaction in $TlBi_2$ increases significantly its electron-phonon coupling constant. As a result, $TlBi_2$, with a logarithmic phonon frequency average one-tenth that of MgB_2, is a phonon-mediated superconductor.

DOI: 10.1103/PhysRevB.108.075203

I. INTRODUCTION

The discovery of phonon-mediated superconductivity in MgB_2 with a transition temperature of 39 K was an important breakthrough in the search for high-temperature superconductivity [1]. Theoretical calculations based on density functional theory suggest that boron p states are dominant near the Fermi level and they form two types of bonds, the in-plane σ bonds between nearest-neighbor (NN) $p_{x/y}$ orbitals and the out-of-plane π bonds between NN p_z orbitals [2–4]. The in-plane σ bonds are strongly coupled to lattice vibrations, resulting in large electron-phonon coupling ($\lambda \sim 1$) and the high superconducting transition temperature ($T_c =$ 39 K). In contrast, the coupling between the p_z-π bonds and high-frequency boron vibrations is relatively weak. The disparity in terms of coupling strength between σ and π bonds leads to the well-known two-gap superconductivity in MgB_2 [4,5].

Since the discovery of MgB_2, there have been efforts to design MgB_2-like superconductors by searching for light-element compounds with p states near the Fermi level. The rationale is that having light elements helps increase phonon frequencies, while having the in-plane σ bonds among p orbitals near the Fermi level enhances electron-phonon coupling strength. Over the years, many MgB_2-like compounds have been discovered and they can be broadly divided into two groups: compounds that crystallize in the MgB_2 structure and compounds that have σ states near the Fermi level. Examples in the former group include vanadium-doped HfB_2/ZrB_2 (8.33/7.31 K) [6], and silicon-doped $YbGa_2$ (2.4 K) [7]. A recent high-throughput study by Yu *et al.* systematically analyzed the structural stability and the electron-phonon coupling of many binary compounds that crystallize in the MgB_2 structure under ambient pressure and several candidate MgB_2-like superconductors were proposed [8]. For the latter group, one prominent example among many others is the hole-doped diamond ($T_c \sim 4$ K) [9–11] which becomes superconducting after the carbon σ bands become partially occupied via hole doping. Finding superconductors by searching for the metallization of σ bands has also inspired a recent study on $La_3Ni_2O_7$ (80 K under pressure) [12].

So far, efforts to design MgB_2-like superconductors are centered around light-element compounds, while compounds that consist of heavy elements are usually considered unfavorable for phonon-mediated superconductivity. However, a recent experiment by Yang *et al.* [13] found that $TlBi_2$ which crystallizes in the MgB_2 structure becomes superconducting below 6.2 K. Given that both Tl and Bi have relatively large atomic masses, superconductivity in $TlBi_2$ is unexpected. Understanding the origin of the superconductivity in $TlBi_2$ is therefore important for future theoretical and experimental searches for MgB_2-like superconductors.

As the atomic number increases, the spin-orbit coupling (SOC) strength increases as well. The atomic numbers of thallium and bismuth are 81 and 83, respectively, which are fairly large. Therefore, the spin-orbit coupling interaction is expected to have important impacts on the electronic structures, the electron-phonon coupling constants, and the topological properties of $TlBi_2$. Lead (Pb), which sits between thallium and bismuth in the periodic table, is known to have a SOC-enhanced electron-phonon coupling constant [14]. Whether SOC has a similar impact on $TlBi_2$ is still unknown and we will explore it in this paper. In addition, SOC is also known to lift band degeneracies and to create topological band composites that could possibly host nontrivial topological states. These topological states are especially important in superconductors because of their potential to host Majorana fermions [15].

*yundi.quan@gmail.com
†zpantz@mail.xjtu.edu.cn

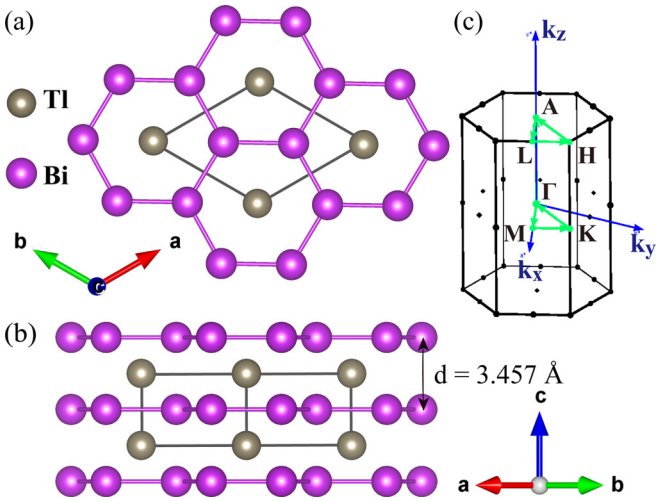

FIG. 1. (a) Top and (b) side view of the crystal structure of $TlBi_2$. (c) Brillouin zone of $TlBi_2$. Bi atoms form two-dimensional honeycomb layers interlaced with Tl atoms.

In this paper, we present a comprehensive first-principles study of $TlBi_2$, in the hope of uncovering the origin of its strong electron-phonon coupling. In addition, the topological properties of $TlBi_2$ are calculated and we point out possible nontrivial topological states in this conventional phonon-mediated superconductor.

II. CRYSTAL STRUCTURE AND METHOD

The intermetallic compound $TlBi_2$ crystallizes in the AlB_2-type structure with Tl interlaced between two-dimensional Bi honeycomb layers, as shown in Figs. 1(a) and 1(b). Its space group is $P6/mmm$ (No. 191) and the calculated lattice constants are $a = 5.749$ Å and $c = 3.457$ Å, which is consistent with experimental parameters [13]. The Tl and Bi atoms occupy $1a$ and $2d$ Wyckoff positions, respectively, namely, Tl : (0, 0, 0), Bi : (1/3, 2/3, 1/2). This crystal structure is known to host high-temperature superconductivity, e.g., MgB_2 (39 K). However, unlike MgB_2 which has a weak interlayer interaction, bismuth atoms in $TlBi_2$ form strong interlayer bonding due to the relatively small c/a ratio.

Density functional theory calculations are carried out using the plane-wave code QUANTUM ESPRESSO [16,17]. The exchange-correlation potential is approximated using the generalized gradient approximation (GGA) as parametrized by Perdew, Burke, and Ernzerhof [18]. We use the optimized norm-conversing pseudopotential proposed by Hamann [19,20]. The kinetic energy cutoff and the charge density cutoff of the plane-wave basis are chosen to be 60 and 240 Ry, respectively. Self-consistent calculations are carried out using a Γ-centered mesh with $24 \times 24 \times 24$ k points and a Methfessel-Paxton smearing width of 0.02 Ry. Structural optimization is performed as well, with the convergence threshold on total energy at 1.0×10^{-7} Ry and that on forces at 1.0×10^{-5} Ry/bohrs.

Phonon dispersions, electron-phonon couplings (EPCs), and superconducting transition temperatures are calculated using the density functional perturbation theory (DFPT) with a $3 \times 3 \times 3$ mesh of q points. Given that both Tl and Bi have large atomic numbers, the spin-orbit coupling (SOC) effect is important. Therefore, calculations both with and without SOC are carried out to help understand the impact of SOC. Wannier functions of Bi $6p$ and Tl $6p$ are constructed to obtain an effective tight-binding Hamiltonian and to study the low-energy physics of $TlBi_2$.

Superconducting transition temperatures of conventional phonon-mediated superconductors can be estimated by using the Allen-Dynes equation [21],

$$T_c = \frac{f_1 f_2 \langle\omega_{\log}\rangle}{1.20} \exp\left(-\frac{1.04(1+\lambda)}{\lambda - \mu^* - 0.62\lambda\mu^*}\right), \quad (1)$$

where f_1 and f_2 are the strong-coupling correction and the shape correction, respectively [21],

$$f_1 = [1 + (\lambda/\Lambda_1)^{3/2}]^{1/3}, \quad (2)$$

$$f_2 = 1 + \frac{(\omega_2/\omega_{\log} - 1)\lambda^2}{\lambda^2 + \Lambda_2^2}, \quad (3)$$

$$\Lambda_1 = 2.46(1 + 3.8\mu^*), \quad (4)$$

$$\Lambda_2 = 1.82(1 + 6.3\mu^*)(\omega_2/\omega_{\log}), \quad (5)$$

The electron-phonon coupling constant λ is

$$\lambda = 2\int \frac{\alpha^2 F(\omega)}{\omega} d\omega, \quad (6)$$

and $\alpha^2 F(\omega)$ is the Eliashberg function which is defined as

$$\alpha^2 F(\omega) = \frac{1}{N_F} \sum \left|g_{mn}^{\nu}\right|^2 \delta(\epsilon_{mk}) \delta(\epsilon_{n,k+q}) \delta(\omega - \omega_{\nu,q}). \quad (7)$$

III. RESULTS

A. Electronic structure

The band structures and the density of states (DOS) of $TlBi_2$ both with and without SOC are shown in Fig. 2. In both cases, the low-energy physics of $TlBi_2$ is dominated by the Bi $6p$ states with a small amount of contribution from the Tl $6p$ states. In the absence of SOC, two bands (four if spin degeneracy is considered), mostly of $p_{x/y}$ characters, become degenerate near −1.8 eV at the Γ point [2]. When the SOC effect is included, the degeneracy at Γ is lifted resulting in a SOC-induced splitting $\Delta_{\rm SOC}^{\Gamma}$ of around 1 eV. Interestingly, the SOC-induced gap opening produces a small gap between band 65 and band 67 in the whole Brillouin zone. In Fig. 2(c), the band structure near the A point in the energy range from −1.3 to −0.7 eV is shown to indicate the SOC-driven gap opening. Although the gap opening due to SOC seems to be small, applying external compressive or tensile strain can effectively increase or decrease the gap, thereby fine tuning the electronic structure of $TlBi_2$.

To identify the topological character of $TlBi_2$, we calculate the Z_2 invariants by assuming a "curved chemical potential" [the red dashed line in Figs. 2(b) and 2(c)] through the gap [15]. The Z_2 topological indices for three-dimensional materials with inversion symmetry can be calculated by inspecting the inversion symmetry operator eigenvalues for the wave functions at the time reversal invariant momenta (TRIM) [22]. In Table I, the parity eigenvalues of $TlBi_2$ for

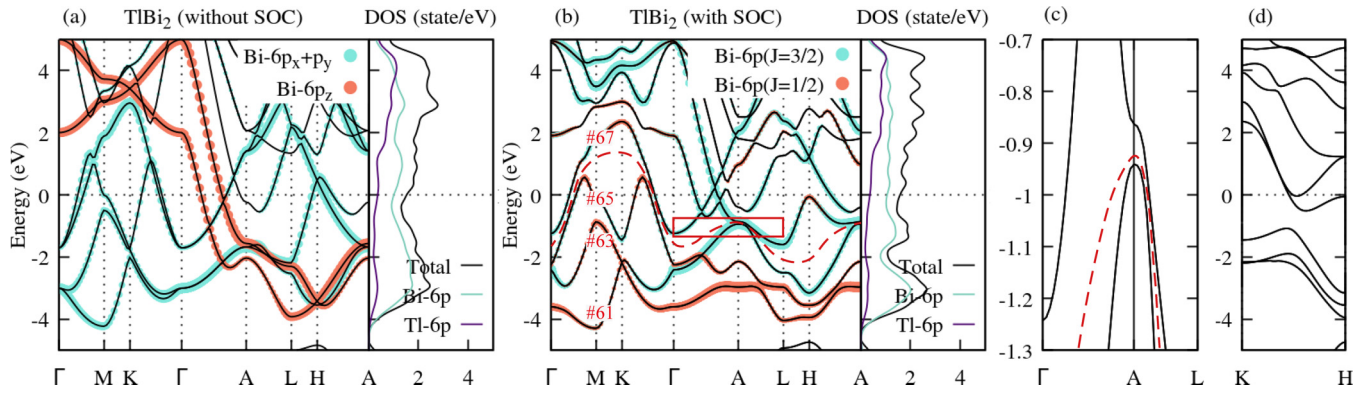

FIG. 2. The electronic band structures and the density of states of $TlBi_2$ (a) without and (b) with SOC. (c) Zoom-in view of the solid red box area in (b). (d) The electronic band structures of $TlBi_2$ with SOC along the K-H path.

bands 61 to 66, along with the Z_2 invariants, are given. The Z_2 invariant of $TlBi_2$ using the curved chemical potential is (1000), which suggests that topologically protected states could exist between band 65 and band 67.

Two studies by Jin *et al.* [23] and Zhou *et al.* [24] reported that the electronic structure of MgB_2 has symmetry-protected nodal lines along $H \rightarrow K$ when the effect of spin-orbit coupling is neglected. The electronic structure of $TlBi_2$ without considering SOC appears to have degenerate states around -2 eV at the K point and 0.2 eV at the H point that could potentially correspond to the nodal line states. However, due to the large spin-orbit coupling interaction in both thallium and bismuth atoms, these degeneracies are lifted [see Fig. 2(d)], and a full gap opens up between band 65 and band 67 at every k point in the Brillouin zone.

B. Fermi-surface nesting

The importance of Fermi-surface nesting in understanding high-temperature superconductivity was discussed extensively in the past [25–27]. It is often noted that large sections of flat regions of Fermi surfaces indicate sharp peaks in the nesting function and consequently large electron-phonon coupling. The Fermi surfaces of $TlBi_2$ without and with SOC are shown in Figs. 3(a)–3(d) and Figs. 3(e)–3(h), respectively, and they are colored by the corresponding orbit weights, from low (blue) to high (red). Although the spin-orbit coupling has a significant impact on the band structures of $TlBi_2$, it nonetheless leaves the Fermi surfaces almost intact.

The Fermi surfaces of $TlBi_2$ consist of three types of surfaces which we label as FS 1, FS 2, and FS 3 [see Fig. 3(a)]. FS 1 has the shape of a hex nut and its orbital character is mostly of Bi $p_x + p_y$ without SOC and $|J = 1/2\rangle$ states when SOC is included. FS 2 has a cylindrical surface in between two flat disks, and it is dominated by Bi $|J = 3/2\rangle$ states as shown in Fig. 3(h) [p_z if SOC is not included; see Fig. 3(d)]. FS 3 seems to have a lotus leaf shape and it is mostly of Bi $|J = 3/2\rangle$ character ($p_{x/y}$ if SOC is not included). Overall, $TlBi_2$ has multiple sections of flat surfaces that are likely to give rise to strong Fermi-surface nesting. We therefore calculate the Fermi-surface nesting function of $TlBi_2$ using the EPW code on a $100 \times 100 \times 100$ k mesh [14,28]. In Figs. 4(a) and 4(b), the nesting functions of $TlBi_2$ on the $k_c = 0$ plane and the $k_a = 0$ plane are plotted. In Figs. 4(c) and 4(d), we plot the nesting function inside the regions in the dashed white boxes in Figs. 4(a) and 4(b). Near the middle point between Γ and M on the $k_c = 0$ plane, there are two nesting function peaks [see Fig. 4(c)], which might originate from FS 1 and FS 2. There are multiple stripes of nesting function peaks on the $k_a = 0$ plane, notably at $k_c = 0.3$ and 0.4. Their origin is likely due to the disk-shaped parts of FS 2 and the flat base of FS 3.

TABLE I. Parity eigenvalues of band 61, 63, and 65 at time reversal invariant points and the product of parity eigenvalues for all the occupied states.

TRIM	Parity	δ	TRIM	Parity	δ
Γ (0, 0, 0)	$++-$	-1	A (0, 0, 1/2)	$-+-$	$+1$
M_1 (1/2, 0, 0)	$-+-$	$+1$	L_1 (1/2, 0, 1/2)	$-+-$	$+1$
M_2 (0, 1/2, 0)	$-+-$	$+1$	L_2 (0, 1/2, 1/2)	$-+-$	$+1$
M_3 (1/2, 1/2, 0)	$-+-$	$+1$	L_3 (1/2, 1/2, 1/2)	$-+-$	$+1$

C. Hopping parameters

To gain a microscopic understanding of the electronic structures of $TlBi_2$, we have obtained the hopping parameters of the states near the Fermi level by calculating the maximally localized Wannier functions (MLWFs) using the WANNIER90 code [29]. The initial projections are chosen to be the Tl and Bi p orbitals. To verify that the Wannier functions can faithfully reproduce the density functional theory (DFT) electronic structures, we compare the Wannier-interpolated band structures with the DFT band structures in Fig. 5 which shows that the interpolated bands are consistent with the DFT results. The Wannier functions that are localized at the Bi atoms are shown in Fig. 6. These MLWFs retain the Bi p-orbital characters, suggesting that hybridization between Bi p states and its neighboring Tl states is weak.

In Table II, the hopping parameters of $TlBi_2$ with SOC and MgB_2 are given. The on-site energies of the bismuth $p_{x,y,z}$ in $TlBi_2$ are around 0.36 eV, while the on-site energies of the boron p_z and $p_{x/y}$ states in MgB_2 are 3.57 and 5.62 eV. Compared with MgB_2, the intralayer σ bonding among Bi $p_{x/y}$ orbitals is slightly weaker. But the interlayer σ hopping between the p_z orbitals of the Bi atoms sitting at different

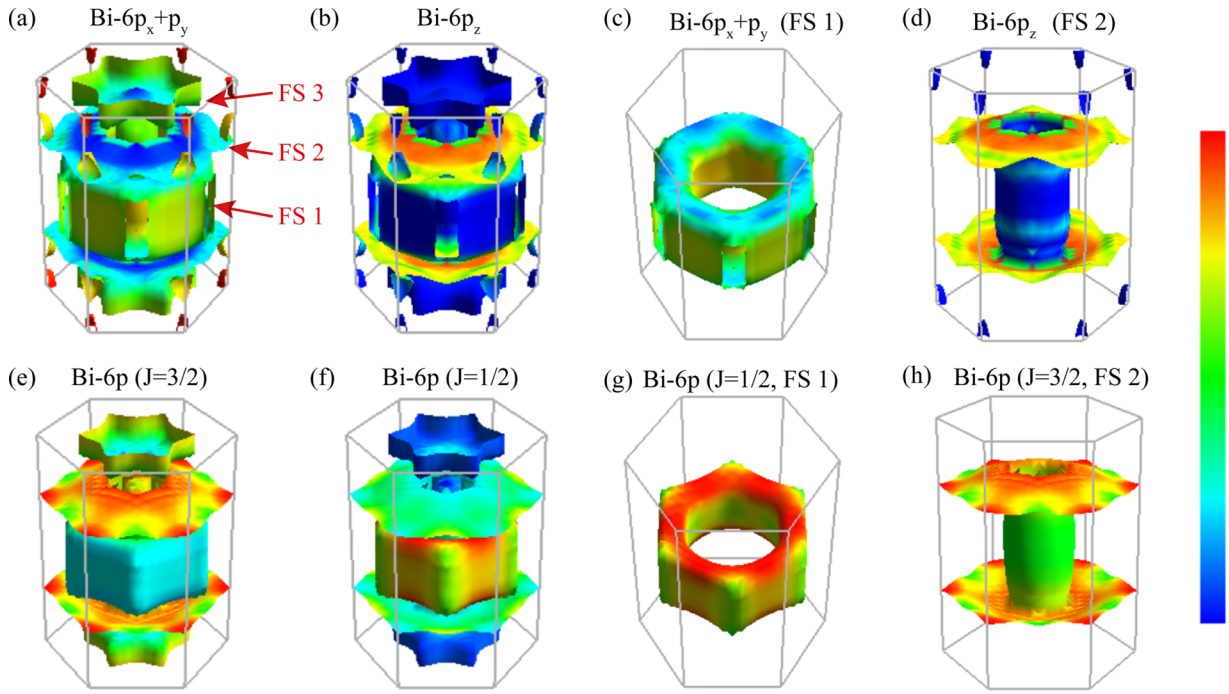

FIG. 3. The Bi *p*-orbital characters of the Fermi surfaces of $TlBi_2$ (calculated without SOC), are presented in (a) and (b), while the relativistic orbital characters of the Fermi surfaces calculated with SOC are presented in (e) and (f). [(c), (d)] and [(g), (h)] show FS 1 and FS 2 without and with SOC, respectively. The intensities of the projected orbitals are indicated by color, from low (blue) to high (red) values.

layers is as large as 1.37 eV, which is in sharp contrast to the negligible interlayer hopping among boron p_z orbitals in MgB_2.

D. Phonon dispersion and electron-phonon coupling

By using the modified McMillan formula, Yang *et al.* estimated the electron-phonon coupling constant of $TlBi_2$ to be

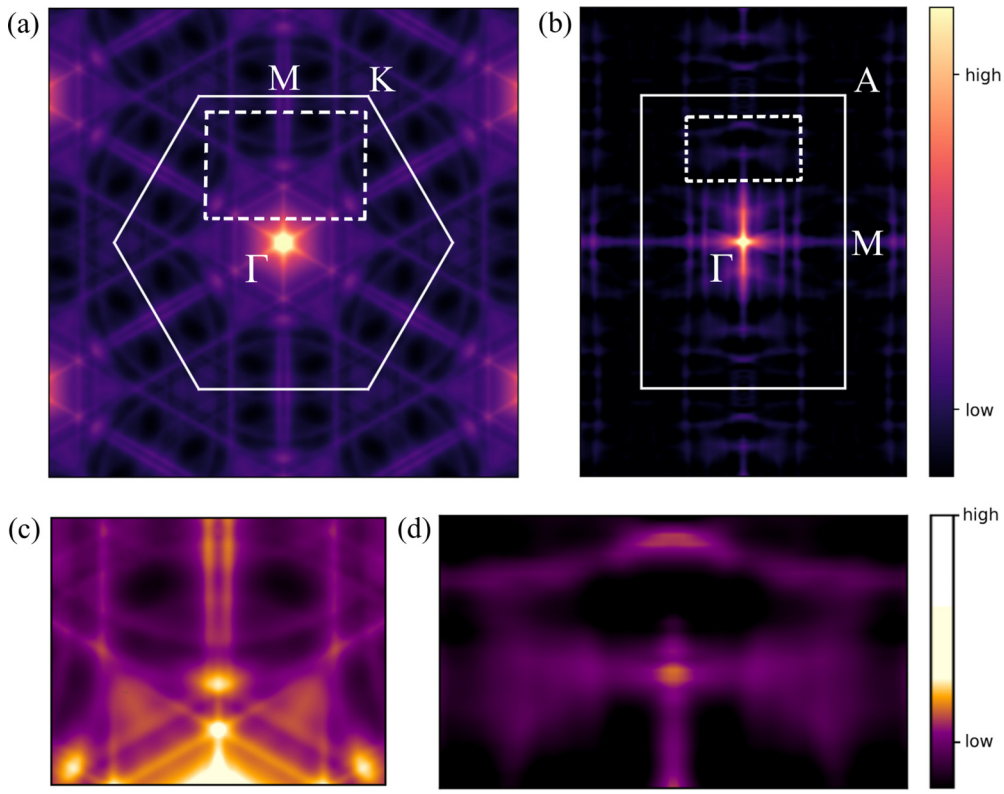

FIG. 4. (a) and (b) are the Fermi-surface nesting functions of $TlBi_2$ on the $k_c = 0$ and $k_a = 0$ planes, respectively. In (c) and (d), the nesting functions inside the dashed white boxes in (a) and (b), respectively, are shown.

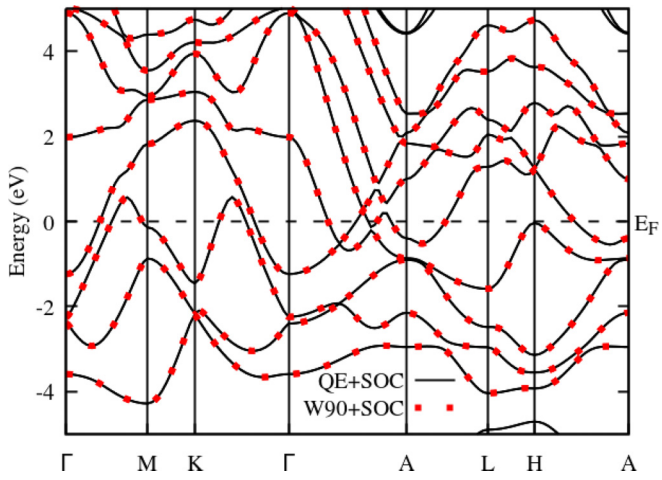

FIG. 5. Band structure of $TlBi_2$ with SOC. Interpolation with WANNIER90 (red dots) and DFT reference band structure (solid black). The Wannier-interpolated band structures are in agreement with the DFT band structures, which indicate that the Wannierzation procedure has converged.

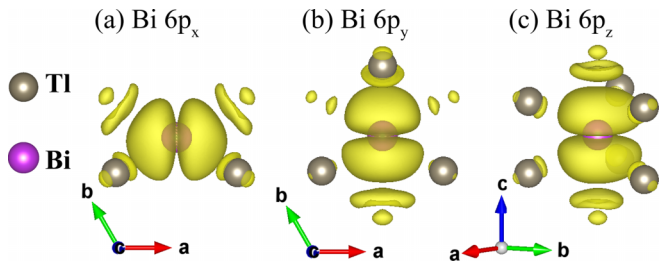

FIG. 6. MLWFs in $TlBi_2$ describing the Bi p orbitals with SOC.

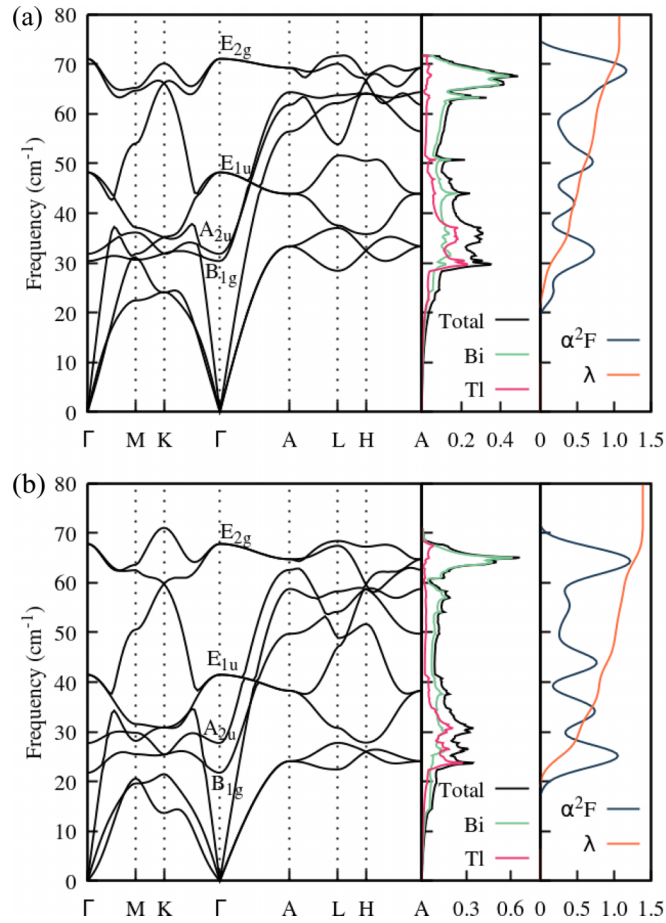

FIG. 7. The phonon dispersion relation, the total and projected phonon density of states (PHDOS), and the Eliashberg function $\alpha^2F(\omega)$ of $TlBi_2$ (a) without and (b) with SOC are shown.

TABLE II. The hopping parameters among X p and M p Wannier orbitals of $TlBi_2$ and MgB_2, where X = Tl, Mg and M = Bi, B. The interlayer σ hopping among the p_z orbitals of the Tl/Bi atoms at different layers of $TlBi_2$ are highlighted in bold, in sharp contrast with the negligible interlayer hopping among the p_z orbitals of the Mg/B atoms in MgB_2.

			Hopping parameter (eV)	
	Wannier orbitals		$TlBi_2$	MgB_2
On-site	X p_z	X p_z	2.79	10.71
	X $p_{x,y}$	X $p_{x,y}$	1.92	8.72
	M p_z	M p_z	0.37	3.57
	M $p_{x,y}$	M $p_{x,y}$	0.36	5.62
Intralayer	M p_x	M p_x	1.15	2.79
	M p_x	M p_y	−0.70	−2.91
	M p_y	M p_y	0.34	−0.53
X-M	X p_z	M p_z	0.30	0.83
	X p_z	M p_y	0.35	1.39
	X p_y	M p_z	0.52	1.54
	X p_y	M p_y	0.87	0.75
Interlayer	X p_z	X p_z	**1.70**	0.05
	M p_z	M p_z	**1.37**	−0.27

around 1.38 [13]. In this paper, we calculate the electron-phonon coupling constant of $TlBi_2$ by running linear-response calculations using the QUANTUM ESPRESSO code. Two calculations, one without SOC and the other with SOC, are carried out. The phonon dispersions, the phonon density of states, and the Eliashberg function $\alpha^2F(\omega)$ without and with SOC are shown in Figs. 7(a) and 7(b), respectively. The Tl phonon partial DOS has the majority of its weight in the 30–40 cm^{-1} range, while Bi vibrations dominate the phonon DOS from 40 to 70 cm^{-1}. Therefore, Tl and Bi atoms are active in different phonon frequency ranges.

At the Γ point, the irreducible representations of the six optical modes are B_{1g} (1), A_{2u} (1), E_{1u} (2), and E_{2g} (2). The integers inside the parentheses indicate the degeneracy of the corresponding phonon mode. In the absence of SOC, the vibrational frequencies of the A_{2u}, B_{1g}, E_{1u}, and E_{2g} modes are around 30, 32, 48, and 71 cm^{-1}, respectively. When SOC is included, the vibrational frequencies of B_{1g}, A_{2u}, E_{1u}, and E_{2g} at the Γ point become 22, 28, 42, and 68 (cm^{-1}), which indicates that the spin-orbit interaction has the effect of phonon softening in $TlBi_2$. As a result, the logarithmic average of the phonon frequencies of $TlBi_2$ decreases from 44 (cm^{-1}) to 37 (cm^{-1}). The electron-phonon coupling constant, on the other hand, increases from 1.1 (without SOC) to 1.4 (with

TABLE III. The structure parameters, the intralayer and interlayer distance of Bi/B atoms, the DOS at the Fermi level $N(E_F)$, λ, $\omega_{\log}$, and T_c for $TlBi_2$ and MgB_2.

	$TlBi_2$		
	w/o SOC	w/ SOC	MgB_2
a (Å)	5.749		3.086
c/a	0.601		1.142
d_{in} (Å)	3.319		1.78
d_{out} (Å)	3.457		3.52
$d_{\text{out}}/d_{\text{in}}$	1.04		1.98
$N(E_F)$ (eV^{-1})	1.5	1.6	0.74
λ	1.1	1.4	0.87
$\omega_{\log}$ (cm^{-1})	44	37	504
T_c (K)	4.4–5.1	5.0–5.5	40
Reference	This paper		[30]

SOC). Using the Allen-Dynes equation and the μ^* ranging from 0.1 to 0.13, we obtain $T_c = 4.4$–5.1 K (without SOC) and 5.0–5.5 K (with SOC).

IV. DISCUSSION AND SUMMARY

In comparison with MgB_2, the logarithmic average of phonon frequencies of $TlBi_2$ is low, about an order of magnitude lower than MgB_2 (see Table III). However, its electron-phonon coupling is as large as 1.4 which helps improve its T_c. Several factors are at play which help enhance the electron-phonon coupling strength of $TlBi_2$ and consequently its T_c. (1) The interlayer Bi-Bi σ bonding among Bi p_z orbitals is strong and it gives rise to large Fermi-surface nesting at a few q_z planes. (2) Although bismuth is heavier than thallium, the phonon modes in the frequency region above 40 cm^{-1} are dominated by Bi vibrations. Also, the phonon modes in this region contribute about one-third of the total electron-phonon coupling strength. (3) The linear-response calculations without and with SOC indicates that SOC can significantly increase the electron-phonon coupling constant λ from 1.1 to 1.4.

Another interesting aspect of $TlBi_2$ is that $TlBi_2$ is a strong topological "insulator" using a curved-chemical-potential approach. The relatively large spin-orbit coupling interaction opens up a small gap between band 65 and band 67 over the whole Brillouin zone, and the size of the gap can be controlled by applying external strain. Given that there is growing interest in studying the topological properties of MgB_2 and similar compounds in recent years [23,24,31–33], $TlBi_2$ could be an interesting candidate for future studies.

ACKNOWLEDGMENTS

This work is supported by National Natural Science Foundation of China Grant No. 11604255 and the Natural Science Basic Research Program of Shaanxi Grant No. 2021JM-001. The computational resources are provided by the HPC center of Xi'an Jiaotong University.

[1] J. Nagamatsu, N. Nakagawa, T. Muranaka, Y. Zenitani, and J. Akimitsu, Nature (London) **410**, 63 (2001).
[2] J. M. An and W. E. Pickett, Phys. Rev. Lett. **86**, 4366 (2001).
[3] A. Y. Liu, I. I. Mazin, and J. Kortus, Phys. Rev. Lett. **87**, 087005 (2001).
[4] H. J. Choi, D. Roundy, H. Sun, M. L. Cohen, and S. G. Louie, Nature (London) **418**, 758 (2002).
[5] S. Souma, Y. Machida, T. Sato, T. Takahashi, H. Matsui, S. C. Wang, H. Ding, A. Kaminski, J. C. Campuzano, S. Sasaki *et al.*, Nature (London) **423**, 65 (2003).
[6] N. Barbero, T. Shiroka, B. Delley, T. Grant, A. J. S. Machado, Z. Fisk, H.-R. Ott, and J. Mesot, Phys. Rev. B **95**, 094505 (2017).
[7] M. Imai, A. Sato, T. Aoyagi, T. Kimura, Y. Matsushita, and N. Tsujii, J. Am. Chem. Soc. **130**, 2886 (2008).
[8] Z. Yu, T. Bo, B. Liu, Z. Fu, H. Wang, S. Xu, T. Xia, S. Li, S. Meng, and M. Liu, Phys. Rev. B **105**, 214517 (2022).
[9] E. A. Ekimov, V. A. Sidorov, E. D. Bauer, N. N. Mel'nik, N. J. Curro, J. D. Thompson, and S. M. Stishov, Nature (London) **428**, 542 (2004).
[10] K.-W. Lee and W. E. Pickett, Phys. Rev. Lett. **93**, 237003 (2004).
[11] L. Boeri, J. Kortus, and O. K. Andersen, Phys. Rev. Lett. **93**, 237002 (2004).
[12] H. Sun, M. Huo, X. Hu, J. Li, Y. Han, L. Tang, Z. Mao, P. Yang, B. Wang, J. Cheng *et al.*, Nature (2023).
[13] Z. Yang, Z. Yang, Q. Su, E. Fang, J. Yang, B. Chen, H. Wang, J. Du, C. Wu, and M. Fang, Phys. Rev. B **106**, 224501 (2022).
[14] S. Poncé, E. Margine, C. Verdi, and F. Giustino, Comput. Phys. Commun. **209**, 116 (2016).
[15] Z. Wang, P. Zhang, G. Xu, L. K. Zeng, H. Miao, X. Xu, T. Qian, H. Weng, P. Richard, A. V. Fedorov *et al.*, Phys. Rev. B **92**, 115119 (2015).
[16] P. Giannozzi, S. Baroni, N. Bonini, M. Calandra, R. Car, C. Cavazzoni, D. Ceresoli, G. L. Chiarotti, M. Cococcioni, I. Dabo *et al.*, J. Phys.: Condens. Matter **21**, 395502 (2009).
[17] P. Giannozzi, O. Andreussi, T. Brumme, O. Bunau, M. B. Nardelli, M. Calandra, R. Car, C. Cavazzoni, D. Ceresoli, M. Cococcioni *et al.*, J. Phys.: Condens. Matter **29**, 465901 (2017).
[18] J. P. Perdew, K. Burke, and M. Ernzerhof, Phys. Rev. Lett. **77**, 3865 (1996).
[19] D. R. Hamann, Phys. Rev. B **88**, 085117 (2013).
[20] M. van Setten, M. Giantomassi, E. Bousquet, M. Verstraete, D. Hamann, X. Gonze, and G.-M. Rignanese, Comput. Phys. Commun. **226**, 39 (2018).
[21] P. B. Allen and R. C. Dynes, Phys. Rev. B **12**, 905 (1975).
[22] L. Fu and C. L. Kane, Phys. Rev. B **76**, 045302 (2007).
[23] K.-H. Jin, H. Huang, J.-W. Mei, Z. Liu, L.-K. Lim, and F. Liu, npj Comput. Mater. **5**, 57 (2019).
[24] X. Zhou, K. N. Gordon, K.-H. Jin, H. Li, D. Narayan, H. Zhao, H. Zheng, H. Huang, G. Cao, N. D. Zhigadlo *et al.*, Phys. Rev. B **100**, 184511 (2019).
[25] C. M. Perlov and C. Y. Fong, Phys. Rev. B **29**, 1243 (1984).

[26] M. D. Johannes and I. I. Mazin, Phys. Rev. B **77**, 165135 (2008).
[27] F. Kaboudvand, S. M. L. Teicher, S. D. Wilson, R. Seshadri, and M. D. Johannes, Appl. Phys. Lett. **120**, 111901 (2022).
[28] F. Giustino, M. L. Cohen, and S. G. Louie, Phys. Rev. B **76**, 165108 (2007).
[29] A. A. Mostofi, J. R. Yates, G. Pizzi, Y.-S. Lee, I. Souza, D. Vanderbilt, and N. Marzari, Comput. Phys. Commun. **185**, 2309 (2014).
[30] Y. Kong, O. V. Dolgov, O. Jepsen, and O. K. Andersen, Phys. Rev. B **64**, 020501(R) (2001).
[31] J. Bekaert, M. Petrov, A. Aperis, P. M. Oppeneer, and M. V. Milošević, Phys. Rev. Lett. **123**, 077001 (2019).
[32] D. Geng, K. Yu, S. Yue, J. Cao, W. Li, D. Ma, C. Cui, M. Arita, S. Kumar, E. F. Schwier, K. Shimada, P. Cheng, L. Chen, K. Wu, Y. Yao, and B. Feng, Phys. Rev. B **101**, 161407(R) (2020).
[33] Y. Zhao, C. Lian, S. Zeng, Z. Dai, S. Meng, and J. Ni, Phys. Rev. B **100**, 094516 (2019).